Twofold origin of strain-induced bending in core-shell nanowires: the GaP/InGaP case

Luca Gagliano[1], Marco Albani[2], Marcel A. Verheijen[1,3], Erik P. A. M. Bakkers[1,4] and Leo Miglio[2] *

[1] Dept. of Applied Physics, Eindhoven University of Technology, 5600 MB Eindhoven, The Netherlands

[2] L-NESS and Dept. of Materials Science, University of Milano Bicocca, 20125, Milano, Italy

[3] Philips Innovation Labs Eindhoven, High Tech Campus 11, 5656 AE Eindhoven, The Netherlands

[4] Kavli Institute of Nanoscience, Delft University of Technology, 2600 GA Delft, The Netherlands

* Corresponding author. E-mail: leo.miglio@unimib.it

Abstract

Nanowires have emerged as a promising platform for the development of novel and high-quality heterostructures at large lattice misfit, inaccessible in a thin film configuration. However, despite core-shell nanowires allow a very efficient elastic release of the misfit strain, the growth of highly uniform arrays of nanowire heterostructures is still a relevant challenge, for instance due to a strain-induced bending morphology. Here we investigate the bending of wurtzite GaP/$In_xGa_{1-x}P$ core-shell nanowires with transmission electron microscopy and energy dispersive X-ray spectroscopy, both in terms of geometric and compositional asymmetry with respect to the longitudinal axis. We compare the experimental data with finite element method simulations in three dimensions, showing that both asymmetries are responsible for the actual bending. Such findings are valid for all lattice-mismatched core-shell nanowire heterostructures based on ternary alloys. Our work provides a quantitative understanding of the bending effect in general, suggesting also a strategy to minimize it.

Keywords: semiconductor nanowire, core-shell, wurtzite, strain, bending

Introduction

Epitaxial heterostructures are a common building block in semiconductor technology for micro- and opto-electronics to enhance device performance. The difference in lattice constants between most semiconductors, however, greatly limits the range of accessible combinations [1]. A lattice mismatch, in fact, strongly promotes the nucleation of detrimental defects, such as misfit dislocations [2]. In this context, core-shell nanowires are of great interest due to both the very small diameter of the core [3] (which can be considered as a compliant substrate) and to the elastic relaxation of the shell in two directions, which is not possible in planar heterostructures [4]. This has been predicted to lead to much lower residual strain and therefore to a higher critical thickness for defect nucleation [5,6]. Therefore, core-shell nanowires do represent a great promise in fabricating novel nanostructures beyond the current technological limits, for example in the fields of solid state lighting [6–8], electronics [9], photovoltaics [10–12] and hydrogen production [13]. Additionally, semiconductor core/superconductor shell nanowire heterostructures have recently gained great attention due to applications in quantum computing and Majorana physics [14]. Lattice mismatch in core-shell nanowires can still lead to unwanted phenomena, such as surface roughness [15], and, for ternary compounds, the formation of compositional inhomogeneities, which could sometimes even result in quantum dots [16]. Despite plastic relaxation can be minimized in nanowires, the residual amount of elastic strain may easily lead to random nanowire bending, hindering the application in array-based devices. This effect has been recently related to one asymmetry in shell thickness by transmission electron microscopy (TEM) [17], which is a time-consuming and, in most cases, destructive technique. In that paper, it is considered highly welcome a 3D simulation taking also into account the possible asymmetry in the shell composition. Actually, a systematic finite element calculation of shell thickness and composition asymmetry for InAsP has been previously considered [18]. Still, despite a comprehensive X-ray diffraction analysis, no comparison between theory and measurements has been performed there, as no experimental access to composition asymmetry was possible.

In such a situation, a diagnostic tool like scanning electron microscopy (SEM), for quickly estimating the degree of both asymmetries in nanowires by measuring the bending, would allow to save time and resources in the optimization of these nanostructures. However, since both the thickness and the compositional asymmetry are to provide bending, a systematic study of both effects is needed.

In this work, we study the strain-induced bending of lattice-mismatched wurtzite (WZ) GaP/$In_xGa_{1-x}P$ core-shell nanowires (NWs) [6,19], using SEM and TEM measurements, performing EDS analysis along with realistic three-dimensional Finite Element Method (FEM) simulations to quantitatively relate the bending to the geometric and to compositional asymmetry. We experimentally investigate and model a representative core-shell NW, accurately mapping its strain condition and comparing the bending to the experimental data. We then extend our model to a set of WZ GaP/$In_xGa_{1-x}P$ samples with varying shell composition and thickness, indicating a predictive procedure to infer the degree of asymmetry of a core-shell NW, by simply measuring its bending curvature.

1. Experimental

1.1. Materials and methods

The nanowires are grown on GaP (111)B substrates, using the Vapor-Liquid-Solid method. The Au catalyst array is fabricated with nanoimprint lithography, with 2.5 μm pitch. WZ GaP nanowires are grown with Metalorganic Vapour Phase Epitaxy (MOVPE) at 615˚C using Trimethylgallium (TMGa) and Phosphine (PH_3) as precursors, while providing Hydrogen Chloride (HCl) to suppress sidewall tapering. Subsequently, ex-situ etching with an Iodine solution is used to remove the Au catalyst. Then a WZ $In_xGa_{1-x}P$ shell is grown by MOVPE, using TMGa, Trimethylindium (TMIn) and PH_3 as precursor gases, following the crystal structure transfer method [20] for WZ GaP/$In_xGa_{1-x}P$ core-shell NWs, as developed in a previous work [6] of ours.

1.2. Results

In Figure 1a-b, we show SEM images of WZ GaP/$In_xGa_{1-x}P$ core-shell NWs with a core diameter of 100nm and a shell of about 40nm, which display a clear bending. The nanowires are bent in different directions with no preferential orientation, as shown in the top view in Figure 1c. Some thin nanowires are curved in two different directions at the same time, resulting in an S-shape. A core-shell NW with sizeable residual strain is actually a metastable system, ready to lower the strain by bending, triggered by any event (e.g. a defect) occurring in a portion of it. As the shell is lattice-mismatched with the core, such a bending is produced by an asymmetry in the corresponding strain, both in shell thickness and composition. This effect is enough to cause bending up to 20 degrees. A simple SEM observation is not enough, at this stage, to gain insight into the actual structure of the nanowires and to assess the origin of bending. We therefore analyse several WZ GaP/$In_xGa_{1-x}P$ NWs by TEM, as shown in Figure 2. In Figure 2a we show the high-angle annular dark-field scanning transmission electron microscopy (HAADF) image of a representative core-shell WZ GaP/$In_xGa_{1-x}P$ NW, clearly demonstrating a strong bending. We see that the wire has two sections: a thicker bottom one (light blue arrow) and a thinner top one (green arrow). Knowing that our WZ GaP NWs are untapered, we deduce that the difference in thickness is caused by the WZ $In_xGa_{1-x}P$ shell. As the thicker part of the NW corresponds to the lower section, we speculate that a larger amount of material was captured by the bottom of the NW than by the top part, due to surface diffusion from the substrate, stopping at some height, possibly due to a surface defect [21].

In Figure 2b-c we show EDS maps in which we can directly observe the thickness and composition asymmetry of the two sections of the nanowire. We report detailed EDS linescans in Figure 2d-e, where the insets describe their position along the nanowire. We summarize the EDS data in Table 1. The apparently lower In concentration at the centre is because the beam penetrates and probes the entire nanowire, which causes also the core to contribute to the measurement. This leads to an underestimation of the In content in the centre of the scan, as this value refers to the entire volume actually probed. The linescan, therefore, yields accurately the

shell composition when only the shell is being probed by the electron beam, which happens at the two peripheral sides of the NW. We notice some relevant differences between the two cross sections of the NW. First, we confirm that the thickness difference is entirely due to the shell itself: in the upper section the shell is approximately symmetric, with a thickness of 40nm on either side. In the bottom section, instead, the shell shows a strong thickness asymmetry, with about 80nm of thickness on the convex side of the nanowire and only about 10nm on the concave one. We notice that the composition of the shell follows the same trend, with the upper section being symmetric within the experimental margin of error (±0.03), while the bottom section of the nanowire shows a strong compositional asymmetry between the two sides. The analysis of the In content in the peripheral part of the shell displays a radial increase, as it is clear in the bottom section. This is likely due to the progressive strain relaxation of the shell with increasing thickness, allowing the hosting of an alloy with a larger lattice parameter, with no increase in the elastic energy.

From these results, we can qualitatively understand the cause of bending in the nanowire: as an initial bending is produced, the lattice constant gets larger on the convex side, generating a more suitable (elastic) chemical potential for the accommodation of the deposited material, increasing both in thickness and in In content. This, in turn, generates a larger load for progressive bending, eventually decreasing the chemical potential and the residual strain in the convex part of the nanowire. Actually, the two asymmetries are related and the lower (elastic) chemical potential on the convex side should both attract more material and be richer in In with respect to the opposite side. The initial bending might be triggered by a random event, for example the formation of an island on the surface of the WZ GaP core, or by some nanometric roughness caused by the Au catalyst etching. This mechanism appears to happen in almost all nanowires, as we have seen in Figure 1. Once an event happens in a random position along the surface of the core, or in the initial stage of the shell, the asymmetric growth is activated, resulting in a random bending degree and orientation. The few S-shaped nanowires are probably caused by two of such events, happening independently in different points, far apart in the longitudinal

direction of the NW. The progressive bending stops when the total thickness of the shell is such that a force balance between the residual strain and the rigidity of the NW is attained.

2. Elastic continuum predictions

2.1. Modeling

In order to perform a quantitative analysis of the strain, and in turn of the bending, by geometric and compositional asymmetry in the NW, we modelled the WZ GaP/$In_xGa_{1-x}P$ core-shell structure by FEM simulations using the COMSOL Multiphysics® software. The anisotropic properties of the elastic constants for WZ crystals are included in the simulation [22,23]. We assume that the lattice constant of WZ $In_xGa_{1-x}P$ follows the empirical Vegard's law for alloys [24], where it varies linearly with composition between the two extremes, represented by the lattice constants of the GaP [25] and InP [26] WZ allotropes. The same procedure is used to interpolate the elastic constants for the WZ $In_xGa_{1-x}P$ alloy [27]. The full 3D structure of the NW is modelled as a core-shell geometry with a regular hexagonal base, where the apothem is considered as the measure of the NW radius. A mechanical equilibrium problem is solved to determine the strain, by imposing a symmetry condition with respect to the middle to simulate a free-standing NW, as it is for the structures analysed by TEM.

In Figure 3a we show a sketch of a strained core-shell NW, presenting a uniform curvature, which we use to illustrate the causes of asymmetry. In Figure 3b-c we show the two types of asymmetry considered. First, shell thickness asymmetry, which we model as a core displacement with respect to the centre of the shell, as shown in Figure 3b. Due to the different thickness, the two sides of the shell will store a different amount of compressive load, higher on the thicker side. The thicker side of the shell will then bend the NW towards the thinner side. Second, we consider the compositional asymmetry, where the composition varies linearly across the shell around an average value, as illustrated in Figure 3c. This compressive load is related to the composition, therefore the side of the shell with the higher In content (higher compression) will bend the NW towards the other side (lower compression), in this case the Ga-rich one.

In Figure 4a we show how the entire NW is modelled, according to the thickness information provided by the microscopy data for a representative case. The NW is divided in three parts: a 2.5μm long top part with 175nm of thickness, a 5.5μm long lower part with 190nm of thickness and a 2μm long central section connecting the two, with linearly varying thickness in order to avoid discontinuities in the simulation. The asymmetric displacement of the core and the asymmetric composition are set according to the experimental data, as reported in Table 1. For the intermediate section of the NW, the displacement of the core, as well as the asymmetry in composition, is modelled as linearly varying across the length, as shown in Figure 4b.

2.2. Results

In the right part of Figure 4a, we show the bent NW resulting from the simulation, where we compare the FEM model on the TEM image of the representative NW, obtaining an excellent agreement. In Figure 4c we show the hydrostatic strain in the nanowire by displaying three cross sections, corresponding to the three different segments. We can see that in all cases the core is, on average, tensile strained (red colour), while the shell is, on average, compressively strained (blue). The distribution of the strain changes across the length of the nanowire, passing from a substantially symmetric distribution, at the top, to a strongly asymmetry in the bottom section. Note that the strain of the core is affected by the asymmetry, showing a compressive strain on the concave side (left) of the bottom section. We see that the shell, in the lower part of the NW, on the convex side (right) of the bottom section is almost completely relaxed in its most peripheral 20nm. The same behaviour is visible in the central section, although less pronounced. This strain relaxation is essentially favoured by the lattice expansion on the right side of the shell, which is provided by the bending of the nanowire toward the left side, as it can be noticed also from the axial strain maps in panel b. From these results we conclude that the strain conditions (and the bending) are directly dependent both from the thickness and compositional asymmetry in the shell.

3. Further Results and Discussion

We now want to understand the relationship between the two asymmetries and the bending in a systematic way, by considering also the influence of the core diameter on the bending. We therefore calculate the NW curvature as a function of core diameter and shell thickness (the average of left and right side thickness) by FEM simulations, for WZ GaP/$In_xGa_{1-x}P$ NW, with average In fraction x=0.25. The simulated nanowires have a compositional asymmetry of x=0.05, therefore opposite facets have In fraction x=0.20 and x=0.30. The thickness is also asymmetric, with a core displacement equal to 1/4 of the shell thickness. The results are shown in Figure 5a, where the colour map quantifies the bending of any nanowire as a function of shell thickness and core diameter. A constant asymmetry along the entire nanowire is now considered for simplicity. It is worth to mention that this analysis is independent on the length of the nanowire, unless it is so small to be of the same order of magnitude of the NW radius. The bending is here quantified as an average curvature by interpolating the NW shape with a parabola and by evaluating the second derivative halfway along the nanowire (see also Figure 5c).

At a fixed shell thickness, we can conclude that the curvature decreases as the core diameter increases. This is because the larger is the core, the stronger is the resistance to the bending induced by the surrounding shell. On the other hand, it is not possible to conclude that the larger is the shell the stronger is the bending. Indeed, if we fix the core diameter, we notice that by increasing the shell thickness we initially observe the bending to increase. This is because the larger volume of the shell can exert a stronger bending force on the core. However, by further increasing the shell thickness, a decrease of the bending is observed, due to a higher stiffness of the total structure of the NW.

Getting back to the FEM results more in details, it is not possible to attribute the bending behaviour as purely dependent on the total NW diameter. This is illustrated in Figure 5b, where the curvature values from panel (a) are plotted as a function of the total nanowire diameter. We see that the curvature is larger for thinner core-shell NW, because it requires less elastic energy.

However, a spreading of the relation between diameter and curvature is observed for larger diameters. To understand this, three curves corresponding to different core diameters are drawn, indicating a complex bending behaviour that can't be related only to the overall nanowire diameter. Indeed, as it was observed in panel (a) at a fixed core diameter, for small shell thickness the bending is intuitively smaller, then it rises up to a maximum, to finally decrease with increasing thickness. This is because the elastic energy needed to bend the nanowire increases with increasing total nanowire thickness, therefore a larger degree of asymmetry is needed to bend a thicker NW than a thinner one. This suggests that a possible strategy to avoid bending in core-shell ternary NWs is to grow graded shells to such a thickness where the stiffness of the nanowire is sufficiently large to prevent bending. Such a strategy is more suitable than starting with a thicker core, as in this case the lower compliance of the latter is likely to produce plastic relaxation by dislocations in the growing shell. We note that since a very good agreement between experimental bending and the one predicted by the simulations (not including any plastic relaxation) is attained, we can conclude that defects do not play an important role for this case of core-shell NW, at least contributing within the experimental uncertainty.

Our aim is now to use these simulation results, in relation to the experimental determination of compositional and geometric asymmetry for a few representative cases, to develop a diagnostic tool for the shell asymmetry of bent nanowires. We do so by collecting the structural parameters of a number of nanowires using TEM, as shown in Figure 5c and reported in Table 2. We compare these data on the shell asymmetry with FEM simulations, where the calculated curvature is reported in a colour map as a function of compositional and thickness asymmetry, obtaining the results displayed in Figure 5d-e, for two different shell thicknesses and compositions. The experimental datapoints are reported as coloured rectangles, where the sides represent the uncertainty, while the colour inside represents the curvature, as measured by the experiments, using the same scale as the FEM colour map in the background. As we can see from both Figure 5d-e and Table 2, the simulation and the experimental data reach an excellent

agreement, demonstrating the FEM modelling as a very accurate predictive tool for the degree of shell asymmetry in a lattice mismatched core-shell nanowire. While the FEM calculations show that the same bending can be obtained either by a very large core shift, with no compositional asymmetry, or by a very large value of the latter, with no core shift, the experimental data indicate that both mechanisms are equally present, being located close to the diagonal of panels (d) and (e). Actually, the two mechanisms are related, since the asymmetry in the shell thickness is produced by a lower chemical potential on the convex side, which is also preferentially attracting the larger In atoms, rather than the Ga ones. In principle, it would be possible to model the kinetic link between the bending stage, i.e. the values of the lattice parameter and the (elastic) chemical potential on the two sides, and the suitable concentrations in a steady state bending configuration, showing that the two asymmetries are clearly linked, as indicated by the experimental data. At present we are not in the position to perform such simulation, however, by supposing a fair equipartition in compositional and thickness asymmetries, it is actually possible to predict the degree of overall asymmetry just on the basis of simple SEM measurements of the NW bending.

4. Conclusions

In this work we quantitatively investigated the origin of bending in WZ GaP/$In_xGa_{1-x}P$ core-shell NWs and developed a predictive tool to estimate the asymmetry of a core-shell NW structure. By measuring the bending in a nanowire, for example by a simple SEM analysis, we can determine a small range in the asymmetry in shell thickness and composition, close to a fair equipartition. Since the curvature is due to such inhomogeneity, this condition should be avoided in those applications, for example quantum wells, where uniformity is required. Therefore, whenever it is compatible with applications, the strategy we propose to avoid bending is to grow a graded buffer shell with composition changing from the same as the core to the desired final composition. In this way, one can allow a gradual elastic strain relaxation due to the nanowire geometry, from one side, and increase the shell thickness to such an extent that bending is more difficult. Due to the elastic relaxation in the buffer shell, it should be also possible to avoid the nucleation of misfit dislocations, giving nanowires a definite advantage over planar geometry hosting lattice-mismatched heterostructures. This work has been developed on WZ GaP/$In_xGa_{1-x}P$ core-

shell NWs, but, in principle, can be extended to any kind of core-shell NW system, provided that the elastic constants of the materials are properly defined, or realistic values can be assumed as in our case.

Acknowledgements

This research is supported by the Dutch Technology Foundation STW and Philips Electronics. STW is part of the Netherlands Organization for Scientific Research (NWO), which is partly founded by the Ministry of Economic Affairs. Solliance and the Dutch province of Noord Brabant are acknowledged for funding the TEM facility. We gratefully acknowledge Roberto Bergamaschini (University of Milano-Bicocca) for accurately reading the manuscript.

References

[1] Shih H-Y, Shiojiri M, Chen C-H, Yu S-F, Ko C-T, Yang J-R, Lin R-M and Chen M-J 2015 Ultralow threading dislocation density in GaN epilayer on near-strain-free GaN compliant buffer layer and its applications in hetero-epitaxial LEDs *Sci. Rep.* **5** 13671

[2] Wang Z, Tian B, Pantouvaki M, Guo W, Absil P, Van Campenhout J, Merckling C and Van Thourhout D 2015 Room-temperature InP distributed feedback laser array directly grown on silicon *Nat. Photonics* **9** 837–42

[3] Vainorius N, Lehmann S, Gustafsson A, Samuelson L, Dick K A and Pistol M-E 2016 Wurtzite GaAs Quantum Wires: One-Dimensional Subband Formation *Nano Lett.* **16** 2774–80

[4] Tatebayashi J, Kako S, Ho J, Ota Y, Iwamoto S and Arakawa Y 2015 Room-temperature lasing in a single nanowire with quantum dots *Nat. Photonics* **9** 501–5

[5] Yan X, Fan S, Zhang X and Ren X 2015 Analysis of Critical Dimensions for Nanowire Core-Multishell Heterostructures *Nanoscale Res. Lett.* **10** 389

[6] Gagliano L, Belabbes A, Albani M, Assali S, Verheijen M A, Miglio L, Bechstedt F, Haverkort J E M and Bakkers E P A M 2016 Pseudodirect to Direct Compositional Crossover

in Wurtzite GaP/In x Ga 1– x P Core–Shell Nanowires *Nano Lett.* **16** 7930–6

[7] Gao Q, Saxena D, Wang F, Fu L, Mokkapati S, Guo Y, Li L, Wong-Leung J, Caroff P, Tan H H and Jagadish C 2014 Selective-Area Epitaxy of Pure Wurtzite InP Nanowires: High Quantum Efficiency and Room-Temperature Lasing *Nano Lett.* **14** 5206–11

[8] Berg A, Yazdi S, Nowzari A, Storm K, Jain V, Vainorius N, Samuelson L, Wagner J B and Borgström M T 2016 Radial Nanowire Light-Emitting Diodes in the (Al x Ga 1– x) y In 1– y P Material System *Nano Lett.* **16** 656–62

[9] Tomioka K, Yoshimura M and Fukui T 2012 A III–V nanowire channel on silicon for high-performance vertical transistors *Nature* **488** 189–92

[10] van Dam D, van Hoof N J J, Cui Y, van Veldhoven P J, Bakkers E P A M, Gómez Rivas J and Haverkort J E M 2016 High-Efficiency Nanowire Solar Cells with Omnidirectionally Enhanced Absorption Due to Self-Aligned Indium–Tin–Oxide Mie Scatterers *ACS Nano* **10** 11414–9

[11] Cui Y, van Dam D, Mann S A, van Hoof N J J, van Veldhoven P J, Garnett E C, Bakkers E P A M and Haverkort J E M 2016 Boosting Solar Cell Photovoltage via Nanophotonic Engineering *Nano Lett.* **16** 6467–71

[12] Mann S A, Oener S Z, Cavalli A, Haverkort J E M, Bakkers E P A M and Garnett E C 2016 Quantifying losses and thermodynamic limits in nanophotonic solar cells *Nat. Nanotechnol.* **11** 1071–5

[13] Standing A, Assali S, Gao L, Verheijen M A, van Dam D, Cui Y, Notten P H L, Haverkort J E M and Bakkers E P A M 2015 Efficient water reduction with gallium phosphide nanowires *Nat. Commun.* **6** 7824

[14] Gazibegovic S, Car D, Zhang H, Balk S C, Logan J A, de Moor M W A, Cassidy M C, Schmits R, Xu D, Wang G, Krogstrup P, Op het Veld R L M, Zuo K, Vos Y, Shen J, Bouman D, Shojaei B, Pennachio D, Lee J S, van Veldhoven P J, Koelling S, Verheijen M A, Kouwenhoven L P, Palmstrøm C J and Bakkers E P A M 2017 Epitaxy of advanced nanowire

quantum devices *Nature* **548** 434–8

[15] Lewis R B, Nicolai L, Küpers H, Ramsteiner M, Trampert A and Geelhaar L 2017 Anomalous Strain Relaxation in Core–Shell Nanowire Heterostructures via Simultaneous Coherent and Incoherent Growth *Nano Lett.* **17** 136–42

[16] Heiss M, Fontana Y, Gustafsson A, Wüst G, Magen C, O'Regan D D, Luo J W, Ketterer B, Conesa-Boj S, Kuhlmann A V, Houel J, Russo-Averchi E, Morante J R, Cantoni M, Marzari N, Arbiol J, Zunger A, Warburton R J and Fontcuberta i Morral A 2013 Self-assembled quantum dots in a nanowire system for quantum photonics *Nat. Mater.* **12** 439–44

[17] Wallentin J, Jacobsson D, Osterhoff M, Borgström M T and Salditt T 2017 Bending and Twisting Lattice Tilt in Strained Core–Shell Nanowires Revealed by Nanofocused X-ray Diffraction *Nano Lett.* acs.nanolett.7b00918

[18] Keplinger M, Kriegner D, Stangl J, Ma˚rtensson T, Mandl B, Wintersberger E and Bauer G 2010 Core–shell nanowires: From the ensemble to single-wire characterization *Nucl. Instruments Methods Phys. Res. Sect. B Beam Interact. with Mater. Atoms* **268** 316–9

[19] Assali S, Zardo I, Plissard S, Kriegner D, Verheijen M a, Bauer G, Meijerink A, Belabbes A, Bechstedt F, Haverkort J E M and Bakkers E P a M 2013 Direct Band Gap Wurtzite Gallium Phosphide Nanowires *Nano Lett.* **13** 1559–63

[20] Algra R E, Hocevar M, Verheijen M a, Zardo I, Immink G G W, van Enckevort W J P, Abstreiter G, Kouwenhoven L P, Vlieg E and Bakkers E P a M 2011 Crystal Structure Transfer in Core/Shell Nanowires *Nano Lett.* **11** 1690–4

[21] Chen C, Plante M C, Fradin C and LaPierre R R 2006 Layer-by-layer and step-flow growth mechanisms in GaAsP/GaP nanowire heterostructures *J. Mater. Res.* **21** 2801–9

[22] Boxberg F, Søndergaard N and Xu H Q 2012 Elastic and Piezoelectric Properties of Zincblende and Wurtzite Crystalline Nanowire Heterostructures *Adv. Mater.* **24** 4692–706

[23] Ferrand D and Cibert J 2014 Strain in crystalline core-shell nanowires *Eur. Phys. J. Appl.*

Phys. **67** 30403

[24] Denton A R and Ashcroft N W 1991 Vegard's law *Phys. Rev. A* **43** 3161–4

[25] Kriegner D, Assali S, Belabbes A, Etzelstorfer T, Holý V, Schülli T, Bechstedt F, Bakkers E P A M, Bauer G and Stangl J 2013 Unit cell structure of the wurtzite phase of GaP nanowires: X-ray diffraction studies and density functional theory calculations *Phys. Rev. B* **88** 115315

[26] Kriegner D, Wintersberger E, Kawaguchi K, Wallentin J, Borgström M T and Stangl J 2011 Unit cell parameters of wurtzite InP nanowires determined by x-ray diffraction *Nanotechnology* **22** 425704

[27] Wang S Q and Ye H Q 2003 First-principles study on elastic properties and phase stability of III–V compounds *Phys. status solidi* **240** 45–54

Figures

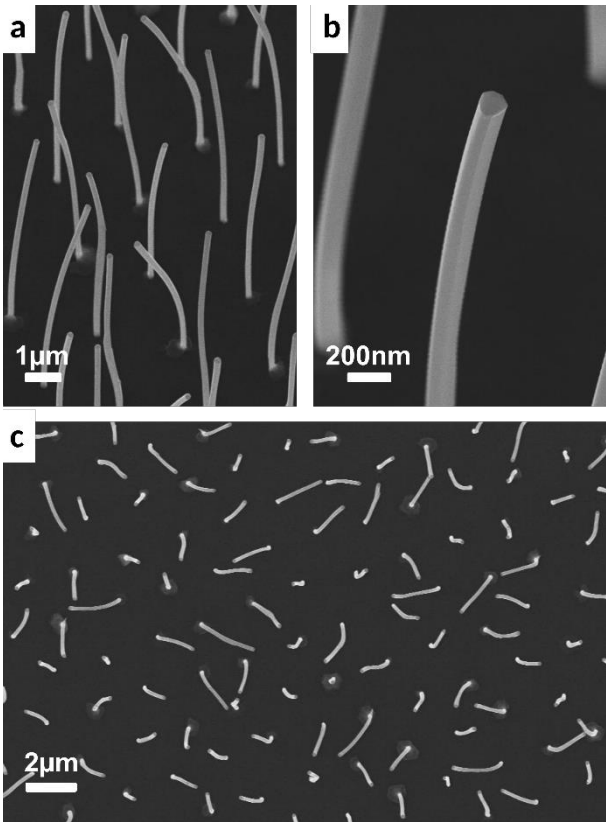

Figure 1. SEM images of WZ GaP/$In_xGa_{1-x}P$ core-shell NWs grown on a zinc-blende (111) GaP substrate. (a) SEM image taken at 30 degrees tilt, showing the clear bending of the nanowires. The nanowires exhibit different degrees of bending, in some cases being bent in two different directions, forming an S-shape, suggesting asymmetry in the core-shell structure developing not only radially, but also axially along the nanowire length. (b) Close-up of a bent WZ GaP/$In_xGa_{1-x}P$ core-shell NW. (c) Top-view SEM image, showing the different bending directions of the nanowires. The degree of bending and the orientation are at random.

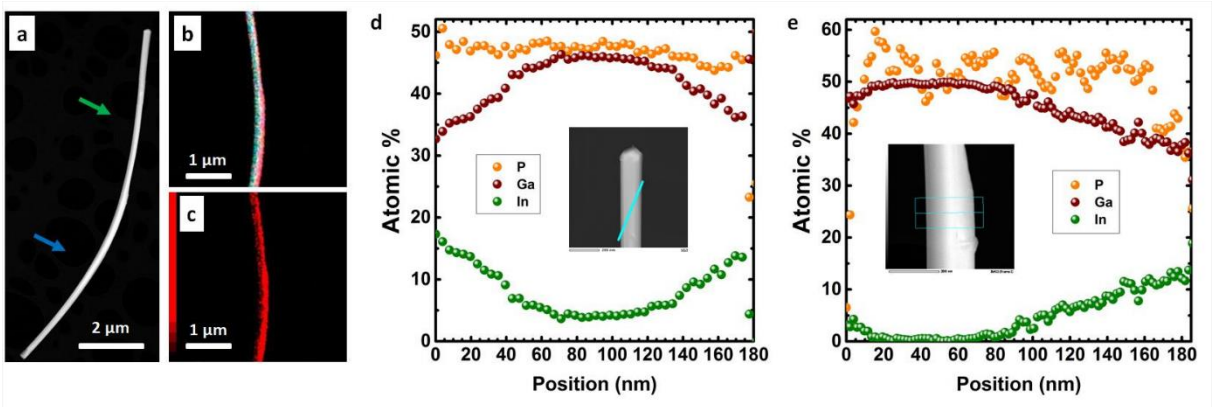

Figure 2. (a) HAADF image of a WZ GaP/$In_{0.2}Ga_{0.8}P$ (average composition) core-shell NW. The nanowire is bent due to strain, given by the lattice mismatch between core and shell. The difference in thickness between the upper and lower section of the nanowire are likely given by a larger flow of material in the lower section due to surface diffusion on the substrate. (b-c) EDS color map of the same nanowire, demonstrating the difference in thickness and composition between the two sections of the nanowire. In (b) we show the signals of both Ga (green) and In (red), while in (c) we show only the In signal to underline the thickness asymmetry. (d-e) EDS linescans of the WZ GaP/ $In_{0.2}Ga_{0.8}P$ core-shell NW in (a-c). The insets indicate the positions where the measurements were taken, where (d) is across the top section of the nanowire, (e) across the bottom section. We notice that the upper section of the nanowire is approximately symmetric, both in thickness and composition, while the bottom section shows both strong thickness and composition asymmetry. The results of these linescans are summarized in Table 1.

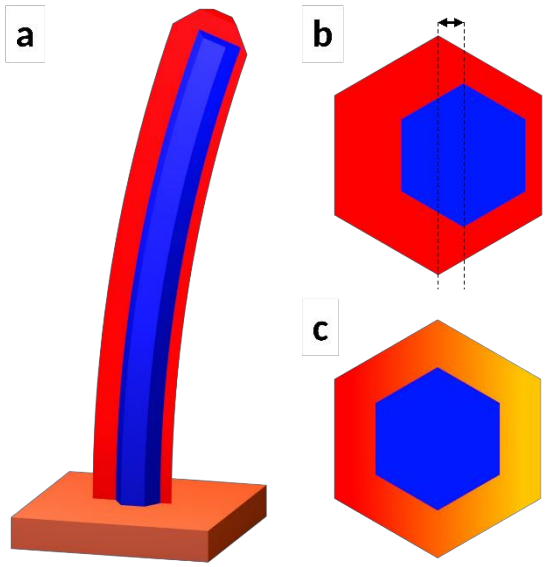

Figure 3. Schematic concept drawing illustrating the structure of the studied nanowires. (a) WZ GaP/$In_xGa_{1-x}P$ core-shell NW. Blue: WZ GaP core. Red: WZ $In_xGa_{1-x}P$ shell. The nanowire is bent due to asymmetry in the shell, which can be of two types. (b) Illustration of thickness asymmetry, which we model as a displacement (shift) of the core with respect to the center of the shell. (c) Illustration of compositional asymmetry, where the orange side represents a lower In composition than the red side. We model the composition as varying linearly between the two sides. Here we define as composition variation the difference between the maximum In composition and the average one.

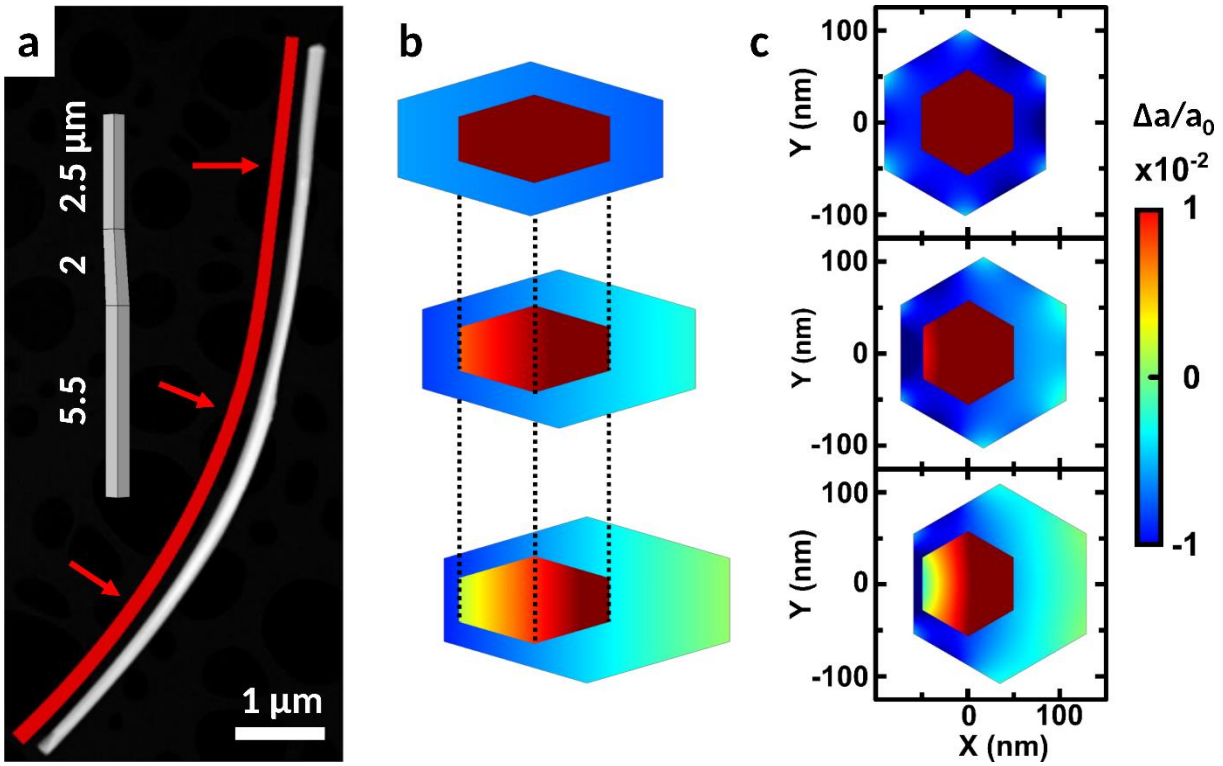

Figure 4. (a) Comparison between FEM simulation (red) and TEM HAADF image of the WZ GaP/$In_{0.2}Ga_{0.8}P$ core-shell NW. The inset shows the three sections used for the FEM simulation. The central section was used to avoid discontinuities in the model. (b) Plots of the axial strain in the three sections of the NW, to illustrate the elastic deformation along the length of the nanowire. The color scale is the same as in panel c. (c) Hydrostatic strain (sum of radial, tangential and axial) plots in the three sections of the NW. The degree of asymmetry in the shell clearly affects the asymmetry in strain distribution. In the bottom section, the left side of the core is subject to compressive strain, while the right side is almost completely relaxed. Only elastic relaxation is considered in the simulation.

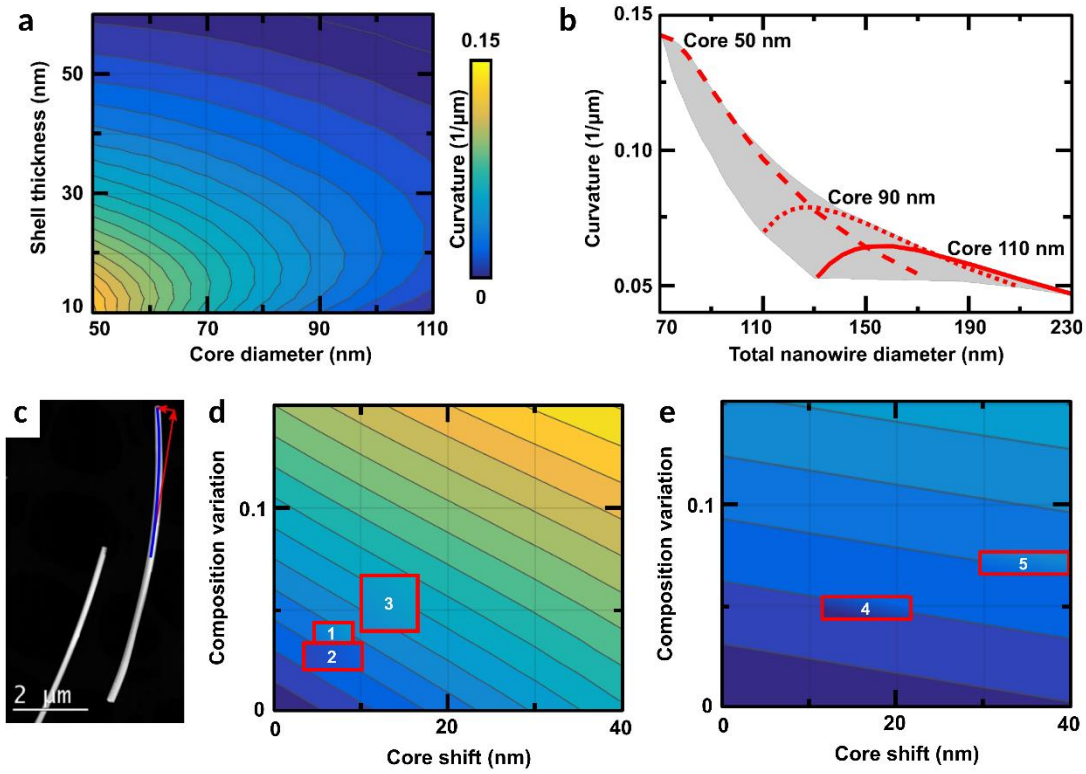

Figure 5. (a) Calculated curvature of a WZ GaP/$In_xGa_{1-x}P$ core-shell NW as a function of the average shell thickness and core diameter. The average composition is fixed to be equal to x=0.25, with a composition variation of ±0.05. The core shift is equal to 1/4 of the shell thickness. The color bar indicates the NW curvature in 1/μm units. (b) Distribution of the nanowire curvature (grey area) as a function of the total nanowire diameter, based on the data from panel (a). The trend does not depend only on the total diameter, but also on the core diameter. The plot of the curvature for three core diameters is outlined by the red curves. (c) HAADF image of two WZ GaP/$In_xGa_{1-x}P$ NWs grown under the same conditions, clearly showing bending. The curvature is measured by interpolating the NW geometry with a parabola (blue line) and by computing the second derivative of this function in the center of the NW. The red arrows are a guide to the eye to indicate the bending-induced displacement of the tip compared to the center of the nanowire. (d-e) Calculated curvature of WZ GaP/$In_xGa_{1-x}P$ NWs as a function of composition and core shift, with overlaid experimental data (red rectangles). The numbers are used to identify the NWs, as reported in Table 2. The color scale representing the curvature is the same as in panel a. The size of each red rectangle represents the experimental error on the two axis dimensions. The color gradient in the rectangle represents the error on the experimental curvature. Parameters: (d) Core 100nm, shell 50nm, average x=0.25. (e) Core

100nm, shell 160nm, average x=0.60. The comparison between calculated and experimental data yields very good agreement.

Tables

Table 1. Structural parameters of the WZ GaP/ $In_xGa_{1-x}P$ core-shell NW shown in Figure 2, obtained by TEM analysis. We report the thickness and the composition of the $In_xGa_{1-x}P$ shell on either side of the NW. The resulting asymmetries cause the bending.

	Thickness left side (nm)	**In fraction left side**	**Thickness right side (nm)**	**In fraction right side**
Top section (experimental)	40±5	0.30±0.04	35±5	0.28±0.04
Bottom section (experimental)	10±5	0.10±0.04	80±5	0.22±0.04
Top section (simulated)	40	0.20	35	0.25
Bottom section (simulated)	10	0.10	80	0.30

Table 2. Experimental data gathered with TEM from the WZ GaP/InGaP core-shell NWs considered in this study. We also compare the measured curvature with the curvature predicted by the FEM simulations. These results are visualized in Figure 5

NW n.	**Composition**	**Shell thickness (nm)**	**Core shift (nm)**	**Composition variation**	**Measured curvature (1/um)**
1	27%	32	6±4	4±2%	0.055±0.01
2	24%	47	7±3	3±1%	0.025±0.01
3	26%	42	12±7	6±3%	0.060±0.01
4	58%	170	17±7	4±1%	0.02±0.01
5	61%	155	35±5	7±1%	0.04±0.01